Efficient Symmetrized DMRG Algorithm for Low-lying Excited States of Conjugated Carbon Systems: Application to Coronene, Ovalene and 1,12-Benzoperylene

Suryoday Prodhan,[1, a)] Sumit Mazumdar,[2, 3, b)] and S. Ramasesha[1, c)]

[1)] *Solid State and Structural Chemistry Unit, Indian Institute of Science, Bangalore-560012, India.*

[2)] *Department of Physics, University of Arizona, Tucson, Arizona 85721, USA.*

[3)] *College of Optical Sciences, University of Arizona, Tucson, Arizona 85721, USA.*

(Dated: 5 January 2016)

Symmetry adapted density matrix renormalization group (SDMRG) technique has been an efficient method for studying low-lying eigenstates in one- and quasi-one dimensional electronic systems. However, SDMRG method had bottlenecks involving construction of linearly independent symmetry adapted basis states as the symmetry matrices in the DMRG basis were not sparse. We have developed a modified algorithm to overcome this bottleneck. The new method incorporates end-to-end interchange symmetry (C_2), electron-hole symmetry (J) and parity symmetry (P) in these calculations. The one-to-one correspondence between direct-product basis states in the DMRG Hilbert space for these symmetry operations renders the symmetry matrices in the new basis with maximum sparseness, just one non-zero matrix element per row. Using methods similar to those employed in exact diagonalization technique for Pariser-Parr-Pople (PPP) models, developed in the eighties, it is possible to construct orthogonal SDMRG basis states while bypassing the slow step of Gram-Schmidt orthonormalization procedure. The method together with the PPP model which incorporates long-range electronic correlations is employed to study the correlated excited state spectrum of coronene, substituted coronene, ovalene and 1,12-benzoperylene; all these systems can be viewed as graphene dots. It is known that in linear polyenes the correlation parameters of the model Hamiltonian determine the ordering of the lowest one-photon, two-photon and triplet states, which are experimentally important. In the systems we have studied, the correlation parameters for all the orbitals of the model are same, however, the ordering of the important states is very different in these systems. This underlines the importance of the topology of the hopping term in the PPP model for molecules. We also discuss in detail the properties of these important states in the molecules we have studied. The properties include bond orders, spin density distribution in the triplet state and transition dipole moment for the low-lying one-photon states from the ground state. Besides, the exciton binding energies and charge gaps are also reported for these systems.

I. INTRODUCTION

Successful exfoliation of a single atomic layer of graphene from graphite crystal has led to an explosion of research, both experimental and theoretical, in the area of graphene and related systems. A sheet of carbon atoms, arranged in honeycomb structure can be assumed to be the parent structure from which carbon allotropes like carbon nanotubes and graphite can be constructed. Each of the carbon atoms in graphene being sp^2-hybridized are σ-bonded with three nearest neighbors while the $2p_z$ orbital, perpendicular to the molecular plain provides the conjugation network. The completely filled σ-band lies deep down in energy and primarily renders stability to the structure. On the other hand, the half filled π-band, due to the overlap of the $2p_z$ orbitals, is mostly responsible for fascinating properties like linear dispersion of electronic energy band near the vertices of

the Brillouin zone leading to formation of Dirac cones. Fractional quantum Hall effect at room temperature and tunneling through classically forbidden region exhibiting Klein paradox are consequences of the dispersion[1].

Being a π-conjugated system, electron-electron correlation should play an important role in the physics of this two-dimensional carbon array, although the strength of correlation may get diminished from well-known π-conjugated systems like polyenes, linear polyacenes or carbon nanotubes due to higher dimensionality. Tight-binding calculations of graphene without explicitly considering the electron-electron repulsion provides sufficiently accurate ground state description[2], yet, ignoring explicit electron correlations has been criticized recently. On the contrary, organic polyene and polyacene systems, which are quasi-one dimensional, have been well studied in the long-ranged Pariser-Parr-Pople (PPP) model and the effect of electron-electron correlation is found to be qualitatively significant. The ordering of excited states in polyenes differ from single CI calculations and it provides an explanation of the optical spectra in these systems[3,4]. Correlation also plays a significant role in dynamical properties of polyenes; observation of electroluminescence efficiency which is far in excess of the upper bound

[a)] Electronic mail: suryodayp@sscu.iisc.ernet.in

[b)] Electronic mail: sumit@physics.arizona.edu

[c)] Electronic mail: ramasesh@sscu.iisc.ernet.in

placed by the spin statistics, gets resolved only after taking explicit electron correlations in account[5]. Crossover of the dipole allowed or one-photon state ($1B_u$) and the dark two-photon state ($2A_g$) in polyacene series with increasing chain length, is observed in the PPP model calculations and agrees well with experiments[6]. Correlated electronic calculations even support the higher optical gaps observed in carbon nanotubes with different diameters, contrary to tight binding calculations[7]. The effect of an additional dimension on the correlation effect, therefore, is worthwhile investigating starting from systems such as polycyclic peri-condensed acenes (graphene nano-discs), which resemble closely to two-dimensional graphene system.

While a number of optical studies have been carried out on polynuclear aromatic hydrocarbons[8], most of the theoretical studies are either in the non-interacting limit or approximating the electron repulsion via a mean field. Moffitt and Coulson calculated the bond order in coronene exploiting both Hückel's tight binding method and valence bond method without considering high energy ionic structures[9] while Pritchard and Sumner calculated the ground state wavefunction and bond order for coronene and ovalene using self-consistent molecular orbital theory[10]. Hummel and Ruedenberg also used similar techniques to study other large polyaromatic hydrocarbons. A number of electronic structure calculations of these polycyclic compounds and their ions, employing density functional theory (DFT) and its time-dependent variant (TDDFT) have been reported[11]. The accuracy of these calculations depend upon the reliability of the functional form of the exchange correlation potential which still is not beyond doubt for strongly correlated systems. Furthermore, implementation of the TDDFT method considers only single particle-hole excitations which lacks the desired accuracy. In recent past, excited state ordering in some of these molecules were studied using multiple reference configuration interaction (MRCI) approach, which considers upto quadruple excitations of each targeted state[12]. The theoretical predictions are in agreement with the optical and two-photon absorption data. Another study has speculated the effect of different molecular geometries over the ordering of excited states in polynuclear hydrocarbons[13]. While the Hartree-Fock semiemperical calculations are oversimplified, the accuracy of the other method used is still dubious. This problem can be overcome by exact diagonalization technique in full Hilbert space, though the size of the Hilbert space increases exponentially with system size and makes it computationally expensive even for moderate-sized systems.

The density matrix renormalization group method (DMRG), put forward by White[14], is a well-accepted method for calculating low-lying states of one and quasi-one dimensional systems. Ramasesha et al. have successfully implemented spatial and discrete symmetries in DMRG to target low-lying states in specific symmetry subspaces[6,15]. In this study, we have employed a new

and highly accurate DMRG algorithm for utilizing end-to-end interchange symmetry (C_2), electron-hole symmetry (J) and spin-flip or parity symmetry (P). The advantage of this algorithm over the previous symmetrized DMRG method is that the symmetry operators can be expressed as highly sparse matrices with only one nonzero element per row. This allows representing the symmetry operators by vectors of the same dimension as of the DMRG Hilbert space. Hence it is possible to employ very large DMRG cut-offs in the new symmetry adaptation algorithm. We have used this new algorithm to calculate the ground state, lowest-lying two-photon and one-photon states in $M_S = 0$ sector along with a few low-lying triplet states in $M_S = 1$ sector for coronene, ovalene, 1,12-benzoperylene and substituted coronene. Notably, coronene has D_{6h} symmetry, while the other three are of lower symmetry groups; nonetheless, in our study, we have considered only one C_2 symmetry axis in all the molecules. We have also characterized these states by calculating bond orders along with the spin density at different sites (in $M_S = 1$ sector). Charge gaps and exciton binding energies for coronene, ovalene and 1,12-benzoperylene are also mentioned here.

The paper is organized as follows. In the next section, we have given an account of the modified algorithm and compared it with exact calculations for 16-site polyene chain and tetracene with 18 p_z-orbitals in conjugation. In section III, we have discussed our results for coronene, ovalene, 1,12-benzoperylene and substituted coronene. In the last section we have summarized our study and concluded.

II. METHODOLOGY

A. Modified Algorithm For Symmetry Adaptation

The DMRG procedure is a truncated Hilbert space algorithm which adopts iterative block-building scheme for calculating low-lying eigenstates of large one or quasi-one dimensional Hamiltonians[14,16]. The system block or left block (L) along with the environment block, also denoted as right block (R) are linearly grown through addition of one new site to each block per iteration and these two together form the superblock which corresponds to the physical system to be studied. In the infinite DMRG algorithm, superblock of size $2l$ consists of system and environment blocks of same size (l). The reduced density matrix of the system (environment) is generated from low-lying eigenstates of the superblock by tracing over the environment (system) states. Matrix elements of the reduced density matrix of the system (environment) are represented by $\rho_{m,m'} = \sum_n \psi_{m,n} \psi^*_{m',n}$, where m, m' are system (environment) states while n are environment (system) states. Reduced density matrices for both the system and environment are diagonalized and M^l density matrix eigenstates (DME) with highest eigenvalues ($\{\mu_L\}$ for system and $\{\mu_R\}$ for environment) are stored as

column vectors of a $M^{l-1}d_\sigma \times M^l$ matrix, where M^{l-1} is the number of truncated reduced density matrix eigenstates retained at $(l-1)$-th iteration and d_σ is the dimension of the Fock space of the newly added site in l-th iteration. The Hamiltonian and site operators of the newly generated blocks are constructed in the basis $\mu^{l-1}\sigma$ and then renormalized using the $M^{l-1}d_\sigma \times M^l$ matrix. Further addition of two new sites gives a system of $2l+2$ sites, whose basis $|\mu_L^l \sigma_i \sigma_{i'} \mu_R^l\rangle$ is generated by direct product of $|\mu_L^l\rangle$ of the system block, $|\mu_R^l\rangle$ of the environment block with $|\sigma_i\rangle$ and $|\sigma_{i'}\rangle$ of the newly added sites to the left and right blocks respectively. The Hamiltonian for the $2l+2$ sites system is formed in this direct product space and diagonalized to get the energy eigenstates, which are utilized for the next iteration. In case of systems with finite size N, finite DMRG algorithm enhances the accuracy in eigenstate calculation; infinite algorithm is employed starting from a small system until the desired superblock size is reached and then sweeping over the superblock is applied by changing the system and environment sizes, keeping the superblock size fixed. The basis at a step of the finite DMRG sweeping can be represented by $|\mu_L^l \sigma_i \sigma_{i'} \mu_R^{N-l+2}\rangle$, where l can vary between 1 and $N-3$. Once the size of the system (environment) block reaches its maximum, the environment (system) block starts to grow at the expense of the other block. A complete sweep consists of expansion of both blocks to their maximum and returning back to the block size of the final infinite DMRG step.

The symmetry elements considered in our modified algorithm are same as in the work by Ramasesha et al.[15]. The C_2 symmetry about an axis perpendicular to the plane of the molecule corresponds to the end-to-end interchange of the superblock with a phase factor:

$$\hat{C}_2|\mu_L^l \sigma_i \sigma_{i'} \mu_R^l\rangle = (-1)^\gamma |\mu_R^l \sigma_{i'} \sigma_i \mu_L^l\rangle$$

or in shorter notation (we will use onwards)

$$\hat{C}_2|\mu\sigma\sigma'\mu'\rangle = (-1)^\gamma |\mu'\sigma'\sigma\mu\rangle$$
$$\gamma = n_\mu(n_\sigma + n_{\sigma'} + n_{\mu'}) + n_\sigma(n_{\sigma'} + n_{\mu'}) + n_{\sigma'}n_{\mu'}$$

i.e. the system and environment blocks interchange their density matrix eigenstates while the two newly added sites also interchange their Fock states. $n_\mu, n_\sigma, n_{\sigma'}$ and $n_{\mu'}$ are the occupancies in the system block, environment block and in the two newly added sites. As the interchange should not affect the superblock Hilbert space, system and environment blocks should have same density matrix eigenspaces. In other words, employing C_2 symmetry approximately halves the effective size of the superblock Hilbert space beside reducing the computational expense by avoiding environment block calculations, at every infinite DMRG step and at the last step of the finite DMRG iteration. In this symmetry operation, each DMRG basis state is carried over to only one unique DMRG basis state, with a phase of ± 1. Thus the C_2 symmetry operation can be stored as a column vector with entry $\pm j_k$, resulting from C_2 operation on the state k.

The Hamiltonian of a half-filled bipartite system conserves electron-hole symmetry (J), where interchanging the creation and annihilation operators at each lattice sites with an associated phase factor keeps the Hamiltonian invariant. On application of this symmetry element, Fock states of a single site transforms in the following way:

$$\hat{J}_i|0\rangle = |\uparrow\downarrow\rangle \qquad \hat{J}_i|\uparrow\rangle = (-1)^{\eta_i}|\uparrow\rangle$$
$$\hat{J}_i|\uparrow\downarrow\rangle = -|0\rangle \qquad \hat{J}_i|\downarrow\rangle = (-1)^{\eta_i}|\downarrow\rangle$$

where η_i is 1 if 'i' belongs to A-sublattice and 0 if it belongs to B-sublattice.

The result of parity or spin-flip symmetry (P) which flips the spin at each site is given by the following:

$$\hat{P}_i|0\rangle = |0\rangle \qquad \hat{P}_i|\uparrow\rangle = |\downarrow\rangle$$
$$\hat{P}_i|\uparrow\downarrow\rangle = -|\uparrow\downarrow\rangle \qquad \hat{P}_i|\downarrow\rangle = |\uparrow\rangle$$

Non-relativistic Hamiltonians remain invariant under parity symmetry. This symmetry can only be employed in $M_S = 0$ space, as application of this symmetry maps from one non-zero M_S space to a $-M_S$ space.

Both J_i and P_i operators are site operators and hence, the operators for the full system can be defined as:

$$\hat{J} = \prod_i \hat{J}_i \qquad \hat{P} = \prod_i \hat{P}_i$$

The matrix element of these two symmetry operators for a superblock of size $2l+2$ can be represented by:

$$\langle\mu'\sigma'\sigma\mu|\hat{\mathcal{R}}_{2l+2}|\nu\tau\tau'\nu'\rangle$$
$$= \langle\mu|\hat{\mathcal{R}}_l|\nu\rangle\langle\sigma|\hat{\mathcal{R}}_i|\tau\rangle\langle\sigma'|\hat{\mathcal{R}}_{i'}|\tau'\rangle\langle\mu'|\hat{\mathcal{R}}_l|\nu'\rangle \tag{1}$$

i.e. it is direct product of matrix elements of corresponding symmetry operators in the left block DME space, right block DME space and in the Fock spaces of the two newly added sites.

The symmetry operators of the superblock follow the relations

$$(\hat{C}_2)^2 = 1 \qquad \hat{J}^2 = (-1)^{(N_s+N_e)} \qquad \hat{P}^2 = 1 \tag{2}$$

where N_s and N_e are number of sites and number of electrons in a basis state, on which the symmetry operations are applied. In case of half-filled fermionic system $N_s = N_e$; subsequently, each of the operator becomes their own inverse, the symmetry operators commute among themselves and form an abelian group. However, the symmetry operators may not commute in individual block spaces and in Fock spaces of newly added sites.

As mentioned earlier, the C_2 symmetry operator maps one direct product state exclusively to another one. However, J and P operators do not produce a single state, due to the absence of one-to-one symmetry correspondence between different density matrix eigenstates of a particular block, although the mapping of Fock states of a single site is exclusive. This absence of one-to-one

mapping of the states in the sub-blocks and hence a one-to-one mapping of the states of the superblock leads to some serious problems in symmetry adaptation. Firstly, the matrix representation of the operators in the DME basis is not very sparse. Secondly, it is difficult to keep track of and thereby include all the symmetry partners of the J and P symmetry while introducing the DMRG cut-off. Thirdly, weeding out linearly dependent states after symmetry adaptation is a slow step as it involves Gram-Schmidt orthonormalization of the symmetrized superblock states. Thus, a successful symmetry adaptation scheme must have a one-to-one unique correspondence between states in the DME basis space.

We invoke the one-to-one correspondence among different DMEs which results in only one non-zero element in each row of the matrices of symmetry operators. This is achieved by considering truncated reduced density matrix eigenstates restricted to a specific region of the Hilbert space, as by symmetry we can obtain the DMEs in the complementary spaces. For example, the DMEs with total number of electrons $n_e < n_s$, the number of sites in the system block, are related to DMEs with $n_e > n_s$ by –

$$\hat{J}_L \mu_i(n_s > n_e) = \mu_j(n_s < n_e) \tag{3}$$

and similarly the DMEs with $M_S > 0$ are related to DMEs with $M_S < 0$ by,

$$\hat{P}_L \mu_i(M_S < 0) = \mu_j(M_S > 0). \tag{4}$$

Hence, we start with the following set of DME of the system block which satisfy the criteria $\{\mu_i(n_s \geq n_e, M_S \leq 0)\}$.

We consider here only the left block, as the algorithm will be same for the right block as well. This particular set of eigenstates can be segregated into four groups –

(i) $\{\mu_\mathbf{i}(\mathbf{n_s} > \mathbf{n_e}, \mathbf{M_S} < \mathbf{0})\}$: Application of J_L, P_L and their product on these eigenstates give the corresponding symmetry counterparts. As J_L and P_L may not commute, we only considered the product $P_L J_L$; the order of operations of the two operators will become irrelevant in the direct product basis space of a half-filled system, where J and P of the superblock commute.

$$\hat{J}_L \ \mu_i(n_s > n_e, M_S < 0) = \mu_{i_J}(n_s < n_e, M_S < 0)$$
$$\hat{P}_L \ \mu_i(n_s > n_e, M_S < 0) = \mu_{i_P}(n_s > n_e, M_S > 0)$$
$$\hat{P}_L \hat{J}_L \ \mu_i(n_s > n_e, M_S < 0) = \mu_{i_{PJ}}(n_s < n_e, M_S > 0)$$

The DMEs obtained from μ_i by symmetry operations are indexed and stored as eigenvectors $\{\mu_i\}$. Symmetry correspondence in every pair of these four eigenstates is also deduced using the relation $\hat{P}_L \hat{J}_L = (-1)^{(n_s+n_e)} \hat{J}_L \hat{P}_L$ along with Eqn. 2 and stored separately. The matrix elements of the symmetry operators are given by,

$$(\hat{J}_L)_{i,j} = (-1)^{\eta_J} \delta_{i,i_J} \qquad (\hat{P}_L)_{i,j} = (-1)^{\eta_P} \delta_{i,i_P}$$

$$(\hat{P}_L \hat{J}_L)_{i,j} = (-1)^{\eta_{PJ}} \delta_{i,i_{PJ}}$$

where ηs are the corresponding phase factors.

(ii) $\{\mu_\mathbf{i}(\mathbf{n_s} > \mathbf{n_e}, \mathbf{M_S} = \mathbf{0})\}$: Application of J_L symmetry operator on these density matrix eigenvectors generate eigenvectors with particle number $2n_s - n_e$; yet, P_L symmetry should map the eigenspace to itself. Therefore, to begin with, this group of eigenvectors is further subdivided into smaller sub-groups $\{\mu_i(n_e = n'_e, M_S = 0)\}$, where n'_e is some particular value of n_e and $n'_e < n_s$. Considering these smaller blocks, one at a time, we set up the matrix of $\hat{P}$ in this sub-space. This is diagonalized to obtain the eigenvectors of $\hat{P}$ so that each of the new DMEs map into themselves with a phase factor of ± 1. These transformed $\mu_k(n_e = n'_e, M_S = 0)$ provide a one-to-one mapping under the symmetry operations $\hat{J}$, $\hat{P}$ and $\hat{P}\hat{J}$.

(iii) $\{\mu_\mathbf{i}(\mathbf{n_s} = \mathbf{n_e}, \mathbf{M_S} < \mathbf{0})\}$: This set of eigenstates are similar to the one discussed above, differing only in the fact that J_L will map the space to itself instead of P_L. The space is sub-divided into smaller blocks on the basis of different negative M_S values and the matrices of the operator $\hat{J}$ are setup in these smaller DME basis spaces. The eigenstates of this operator serve as the new DMEs for obtaining one-to-one correspondence of the DMEs under the symmetry operations.

(iv) $\{\mu_\mathbf{i}(\mathbf{n_s} = \mathbf{n_e}, \mathbf{M_S} = \mathbf{0})\}$: This particular set of eigenvectors span a vector space which on application by both J_L and P_L should map into itself. Hence, linear combinations are found out which are eigenvectors of J_L with eigenvalues $(-1)^{\zeta_J}$, $\zeta_J = 0$ or 1. Using J-eigenvectors with a particular eigenvalue $(-1)^{\zeta_J}$, another set of linear combinations are formed which are eigenvectors of P_L, with eigenvalues $(-1)^{\zeta_P}$, $\zeta_P = 0$ or 1. To this end, we first construct the matrix representation of $\hat{J}$ in the basis of DMEs with $n_s = n_e$ and $M_S = 0$. We obtain the eigenvectors of $\hat{J}$ in this space by diagonalizing the matrix. We then use the eigenvectors of $\hat{J}$ as the basis in which the matrix of $\hat{P}$ is set up. The resulting eigenvectors of $\hat{P}$ replace the DMEs in this space and they will be employed in symmetry adaptation.

While imposing the cut-off in the DMEs, we only consider the subspace of DMEs with $n_e \leq n_s$ and $M_S \leq 0$. Since the DMEs related to these states by the operation of $\hat{J}$, $\hat{P}$ and $\hat{P}\hat{J}$ will also have the same eigenvalues, it is ensured that all DMEs above a cut-off in the density matrix eigenvalue are included. Usually the cut-off imposed in the specified sector is about 0.4 times of the cut-off intended for the full density matrix. Since we have a one-to-one correspondence of the DMEs within a block for the operations $\hat{J}$, $\hat{P}$ and $\hat{P}\hat{J}$, it is a simple matter to extend the one-to-one correspondence to the direct product basis states formed by the DMEs of the left and right blocks and the Fock space states of the newly added sites.

Symmetry adapted direct product bases in an irreducible representation Γ can be generated by employing projection operator, which is given by –

$$\mathcal{P}(\Gamma) = \frac{1}{h} \sum_i \chi(\Gamma, \mathcal{R}_i) \hat{\mathcal{R}}_i \tag{5}$$

where $\chi(\Gamma, \mathcal{R}_i)$ is the character of the symmetry operator $\hat{\mathcal{R}}_i$ in the irreducible representation Γ and h being the order of the group. Operation by $\mathcal{P}(\Gamma)$ on each of the basis states in the direct product space produces the symmetry adapted linear combinations. However, if $\mathcal{P}(\Gamma)$ acts on each of the states in the direct product space, we will end up with a linearly dependent symmetry adapted basis. In the earlier symmetry adaptation procedure[15], weeding out linear dependence by Gram-Schmidt orthonormalization technique was an extremely expensive step, computationally. With present technique, where we have a one-to-one correspondence between symmetry related states, this turns out to be extremely simple and computationally very efficient. Firstly we note that, one-to-one correspondence between the DMRG basis states under the symmetry operations implies that a given basis state can appear only once (or not at all) in a given symmetry space. Therefore, in the symmetry adaptation step, we sequentially go through the list of basis states, apply the projection operator and construct the symmetrized combination along with elimination of the partners which have appeared in the symmetry combination from the list of unsymmetrized basis states. This ensures that a basis state occurs at most once in the symmetrized states. Taken together with the orthonormality of the unsymmetrized basis states, this ensures orthogonality of the basis states generated by the projection operator. Using these symmetry combinations, we can generate the transformation matrix S, which is $D \times D_\Gamma$ matrix where D is the dimensionality of the unsymmetrized space and D_Γ is the dimensionality of the symmetrized space.

The Hamiltonian of the superblock can be transformed into symmetrized basis space by operating with the matrix S as:

$$\tilde{H}_{2l+2} = S^\dagger H_{2l+2} S \tag{6}$$

The transformed Hamiltonian is then diagonalized to get lowest-lying eigenvectors in different irreducible representations labeled as $^eA^+$, $^eB^+$, $^eA^-$, $^eB^-$, $^oA^+$, $^oB^+$, $^oA^-$ and $^oB^-$, where the left-hand superscript represents character under P-symmetry, the right superscript is the character under J-symmetry and the letter A/B is the character under C_2 symmetry in the irreducible representation Γ. The singlet lies in the 'e' space while the triplet lies in the 'o' space. The space '+' refers to 'covalent' space while '-' to the 'ionic' space. $A(B)$ represents the space even (odd) under C_2 symmetry. The ground state is usually in $^eA^+$ while the optically connected space is $^eB^-$. The lowest triplet lies in the $^oB^+$ space.

B. Model Hamiltonian

The model Hamiltonian employed for the study of peri-condensed polyacenes is the well known Pariser-Parr-Pople (PPP) Hamiltonian[17], which considers long-range Coulombic interaction along with on-site Hubbard interaction:

$$
\begin{aligned}
H = &\sum_{<i,j>,\sigma} t_0(\hat{c}_{i,\sigma}^\dagger \hat{c}_{j,\sigma} + \text{ H.C.}) + \sum_i \epsilon_i \hat{n}_i \\
&+ \sum_i \frac{U}{2}\hat{n}_i(\hat{n}_i - 1) + \sum_{i>j} V_{ij}(\hat{n}_i - z_i)(\hat{n}_j - z_j)
\end{aligned}
\tag{7}
$$

t_0 is the nearest-neighbor hopping integral between bonded sites 'i' and 'j', ϵ_i is the site energy of 'i'-th carbon atom while U is the on-site Coulomb repulsion term. The intersite interaction energies, V_{ij} are interpolated by Ohno scheme[18] assuming C-C bond length of 1.4 Å. $\hat{c}_{i,\sigma}^\dagger$ and $\hat{c}_{i,\sigma}$ are the creation and annihilation operators of an electron with spin σ in the $2p_z$ orbital of the carbon atom at site 'i' and $\hat{n}_i = \sum_\sigma \hat{c}_{i,\sigma}^\dagger \hat{c}_{i,\sigma}$ is the corresponding number operator. For carbon atoms, the standard PPP parameters are $t_0 = -2.4$ eV and $U = 11.26$ eV while the site energy (ϵ) for unsubstituted carbon atom is taken to be zero. z_i is the local chemical potential, expressed by the the number of electrons at site 'i' which leaves the site neutral; for carbon atoms in a π-conjugated system, $z_i = 1$. Substitution effect by donor or acceptor groups can be modeled by considering the site energy ϵ_i positive or negative respectively.

As DMRG calculations are done in constant M_S-basis space, contrary to the spin-adapted basis (Diagrammatic valence bond basis) calculations, labelling states by their spin value is ambiguous. The parity symmetry partially resolves this as the singlet state lies in the even-parity subspace while the triplet state lies in the odd-parity subspace. Though, higher spin states also lie in the even (odd) parity sub-spaces, they remain high in energy compared to singlet and triplet states in moderate sized carbon-based systems and so can be neglected[6].

C. Comparison with exact calculation results

The accuracy of our modified algorithm can be established by comparing the results obtained for small systems with exact PPP results, like in 16-site polyene chain and tetracene molecule which has 18 sites. The difference between ground state energy of 16-site polyene chain, obtained by symmetrized DMRG technique, and the exact calculation result is plotted for four different cutoff values M'^l in the sector $\{\mu_i^L(n_s \geq n_e, M_S \leq 0)\}$ of the sub-block in Fig. 1. In all the calculations, the energy values are accurate at least up to fifth decimal places when compared with exact calculation results. We have also plotted the fluctuations in the DMRG energy about the exact energy with number of finite DMRG sweeps for a fixed M'^l value, which depicts that the fluctuation is negligible with number of sweeps and therefore, $2-3$ sweeps will suffice for acceptable convergence of energy.

In Table I, PPP energies of the ground state (1^1A^+), lowest two-photon state (2^1A^+), lowest one-photon state (1^1B^-) and of the lowest triplet state (1^3B^+) of both 16-site polyene chain and tetracene molecule are presented.
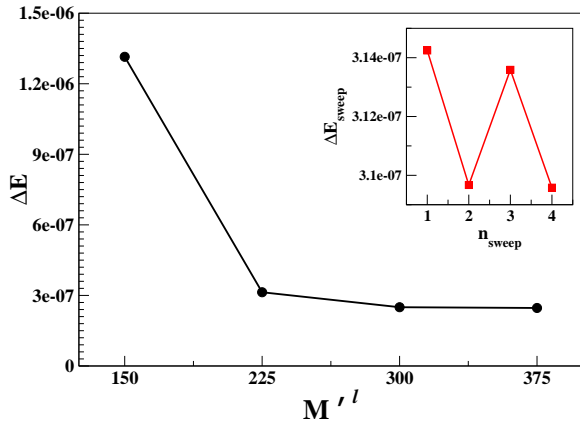
FIG. 1. (Color online) Deviation of ground state energy calculated by symmetrized DMRG technique from exact energy value for different cutoff M'^l of the density matrix eigenstate space. The number of finite DMRG sweeps (2) is fixed in all the cases. Inset: Fluctuation of DMRG ground state energy with respect to exact energy value with increasing number of finite DMRG sweeps. The number of density matrix eigenstates retained, M'^l, is 225.
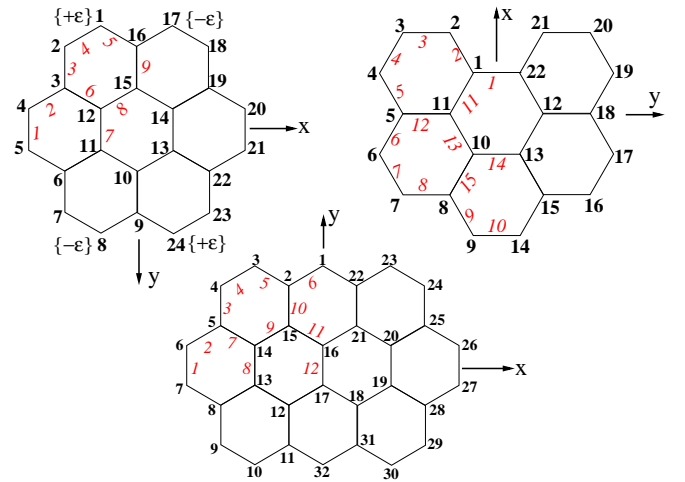

FIG. 2. (Color online) Schematic diagrams of coronene, 1,12-benzoperylene and ovalene with site (black and bold) and bond (red and italics) indices. The sites of substitution in substituted coronene are indicated in curly brackets; $+\epsilon$ (sites 1 and 24) represents a donor site while $-\epsilon$ (sites 8 and 17) represents an acceptor site.

M'^l is kept at 225 for 16-site polyene chain and 425 for tetracene molecule, thus total number of DMEs retained for the sub-block is ~ 550 and ~ 1000 respectively at each step of DMRG calculation. Full CI calculations, employing diagrammatic valence bond method (DVB)[19], shows excellent agreement with the results obtained and the upper bound of error in energies of different states is of the order of 10^{-4}.

TABLE I. Comparison of the energies of ground state, lowest two-photon state, lowest optical state and lowest triplet state of 16-site polyene chain and tetracene, obtained by modified symmetrized DMRG algorithm and exact calculation. The exact calculations are carried out using diagrammatic valence bond method.

System	State	Exact calculation	DMRG calculation
Polyene of	1^1A^+	-33.55575	-33.55575
16 sites	2^1A^+	-32.03385	-32.03385
	1^1B^-	-30.43291	-30.43291
	1^3B^+	-32.87993	-32.87993
Tetracene	1^1A^+	-43.69083	-43.69076
molecule	2^1A^+	-40.55749	-40.55725
	1^1B^-	-40.51439	-40.51419
	1^3B^+	-42.47046	-42.47038

III. RESULTS AND DISCUSSION

We have studied a few low-lying states of coronene, ovalene and $1,12-$benzoperylene in different symmetry spaces considering ~ 1000 DMEs in PPP model and the energy gaps are tabulated in Table. II and III. We have also calculated energies in the above symmetry spaces for substituted coronene, with donor and acceptor groups of equal strength, set to 1.0 eV ($|\epsilon| = 1.0$ eV). We have employed only a few of the existing spatial symmetries of the molecules, namely C_2 symmetry axis perpendicular to the molecular plane (in plane C_2 axis in case of $1,12-$benzoperylene) for our calculations, as our DMRG calculations cannot incorporate more than one symmetry axis. Being treated as planar molecules, with Wannier orbitals, the reflection in the molecular plane is a trivial symmetry. Yet, we can label the eigenstates according to different irreducible representations of the full group based on transition dipole moment direction for excitations from the ground state. In case of coronene, we have considered its subgroup D_{2h} rather than the full group D_{6h} for labelling the eigenstates. The lowest optical states obtained may not be the states with highest transition dipole moment, which will be prominent in UV-visible spectroscopy but corresponds to the lowest energy state of the appropriate symmetry subspace; however, the results obtained are in good agreement with gas phase molecular spectroscopic data available for above molecules[8], suggesting that the states obtained are also the ones with considerable transition dipoles in the energy range of the experiment.

The relative ordering of the energy levels are closely associated with the effective correlation strength in lin-

TABLE II. Lowest energy states in coronene and ovalene with the energy gaps in units of eV. Although coronene has D_{6h} symmetry, here the energy states are labelled according to Abelian D_{2h} symmetry representations. The transition dipole moment from ground state to the excited states ($\mu_{tr,x/y}$) along specific axes are also specified in the last two columns in units of Debye.

Nature of the state	State level	Energy Gap	$\mu_{tr,x}(D)$	$\mu_{tr,y}(D)$
Coronene				
Two-photon	$(2\,^1A_g^+/1\,^1B_{1g}^+)^a$	3.97	0.00	0.00
	$(3\,^1A_g^+/2\,^1B_{1g}^+)$	4.09	0.00	0.00
	$(4\,^1A_g^+/3\,^1B_{1g}^+)$	5.08	0.00	0.00
Optical	$1\,^1B_{2u}^-$	4.83	0.81[b]	8.43
	$1\,^1B_{3u}^-$	4.87	7.51	0.49
Triplet	$(1\,^3B_{2u}^+/1\,^3B_{3u}^+)$	2.35	0.00	0.00
	$(2\,^3B_{2u}^+/2\,^3B_{3u}^+)$	3.00	0.00	0.00
	$(3\,^3B_{2u}^+/3\,^3B_{3u}^+)$	3.02	0.00	0.00
	$(1\,^3A_g^+/1\,^3B_{1g}^+)$	3.35	0.00	0.00
Dark states	$(1\,^1B_{2u}^+/1\,^1B_{3u}^+)$	2.82	0.00	0.00
	$(x\,^1B_{2u}^-/\ x\,^1B_{3u}^-)^c$	3.88	0.28	1.74
	$(1\,^1A_g^-/1\,^1B_{1g}^-)$	4.73	0.00	0.00
Ovalene				
Two-photon	$(2\,^1A_g^+/1\,^1B_{1g}^+)$	3.10	0.00	0.00
	$(3\,^1A_g^+/2\,^1B_{1g}^+)$	3.75	0.00	0.00
	$(4\,^1A_g^+/3\,^1B_{1g}^+)$	5.48	0.00	0.00
Optical	$1\,^1B_{2u}^-$	3.32	0.29	6.58
	$2\,^1B_{2u}^-$	4.53	0.33	0.58
	$1\,^1B_{3u}^-$	4.64	7.28	0.22
Triplet	$(1\,^3B_{2u}^+/1\,^3B_{3u}^+)$	1.49	0.00	0.00
	$(1\,^3A_g^+/1\,^3B_{1g}^+)$	2.77	0.00	0.00
	$(2\,^3A_g^+/2\,^3B_{1g}^+)$	2.80	0.00	0.00
	$(2\,^3B_{2u}^+/2\,^3B_{3u}^+)$	2.82	0.00	0.00
Dark states	$(1\,^1B_{2u}^+/1\,^1B_{3u}^+)$	2.65	0.00	0.00
	$(1\,^1A_g^-/1\,^1B_{1g}^-)$	4.06	0.00	0.00
	$(2\,^1A_g^-/2\,^1B_{1g}^-)$	4.69	0.00	0.00

[a] Probable labels for states which cannot be identified uniquely are given within parentheses.

[b] Non-zero value of transition dipole moment along polarization direction forbidden by symmetry is an artifact of the calculations as average density matrices, calculated from eigenstates of different symmetry subspaces, are employed to determine the transition dipole moment. However, the errors are negligible as intensities depend on the square of the transition dipole moment.

[c] x implies that the level numbering is unknown.

ear $\pi-$conjugated systems. In extended systems effective correlation strength can be thought of as the ratio of the on-site PPP correlation to the bandwidth of the one-particle spectrum. However, in molecules with discrete excitation spectrum, it is difficult to use the width of the energy spectrum in place of the band width. Thus, it is difficult to a priori predict the ordering of the states based on one-particle bandwidth which are similar in all the molecules we have studied. In PPP or extended Hubbard model, the on-site correlation strength to a first approximation is expressed by $U_{PPP} \sim (U - V_{12})$, where V_{12} is the nearest-neighbor PPP term. Our calculations yield the lowest two-photon gap in ovalene molecule to be almost twice that of the lowest spin gap, which is a

TABLE III. Lowest energy states in 1,12-benzoperylene and substituted coronene with the energy gaps in units of eV. The transition dipole moment from ground state to the excited states ($\mu_{tr,x/y}$) along specific axes are also specified in the last two columns in units of Debye.

Nature of the state	State level	Energy Gap	$\mu_{tr,x}(D)$	$\mu_{tr,y}(D)$
1,12-Benzoperylene				
Two-photon	$2\,^1A_1^+$	2.99	0.00	0.00
	$3\,^1A_1^+$	4.26	0.00	0.00
	$4\,^1A_1^+$	4.58	0.00	0.00
Optical	$1\,^1B_1^-$	3.72	0.00	3.17
	$2\,^1B_1^-$	4.71	0.00	3.83
	$3\,^1B_1^-$	4.83	0.00	5.20
Triplet	$1\,^3B_1^+$	2.84	0.00	0.00
	$2\,^3B_1^+$	3.65	0.00	0.00
	$3\,^3B_1^+$	4.26	0.00	0.00
Substituted coronene				
Two-photon	$2\,^1A_g$	4.01	0.00	0.00
	$3\,^1A_g$	4.81	0.00	0.00
	$4\,^1A_g$	4.90	0.00	0.00
Optical	$1\,^1B_u$	2.90	0.00	0.23
	$2\,^1B_u$	3.87	0.12	1.46
	$3\,^1B_u$	5.18	0.17	7.52
	$4\,^1B_u$	5.97	4.10	0.59
Triplet	$1\,^3B_u$	2.29	0.00	0.00
	$2\,^3B_u$	2.92	0.00	0.00
	$3\,^3B_u$	3.48	0.00	0.00

characteristic feature of regular polyene systems where two-photon state is predominantly two triplet excitations. The other two molecules and substituted coronene, on the other hand, do not show this signature. Therefore, it can be suggested that the effective electronic correlation strength in ovalene molecule is comparable to regular polyene systems while the $\pi-$ electrons in other molecules are less correlated. The ordering of low-lying singlet excited states in coronene and ovalene, although, are in accordance with those in strongly correlated systems; the lowest optical states lie above the lowest two-photon states in both the systems. However, 1,12-benzoperylene shows some peculiar trend as the lowest two-photon state remains close to the lowest triplet state and quite low in energy compared to $1\,^1B_1^-$, showing that in this system, we cannot view the $2\,^1A_1^+$ state as made up of two triplets generated in different parts of the molecule.

The lowest two-photon gaps along with the lowest triplet gaps calculated in coronene and ovalene are in excellent agreement with the earlier report by Aryanpour et al.[13]. The two-photon gaps reported earlier are 3.96 eV and 3.03 eV respectively for these systems, against 3.97 eV and 3.10 eV, found in our calculations. The triplet gaps earlier reported are 2.38 eV and 1.57 eV for coronene and ovalene respectively, which are close to 2.35 eV and 1.49 eV obtained by us. However, the lowest one-photon gaps and relative positions of the lowest optical states with respect to the lowest two-photon states do not agree well with the previous study. In coronene, the lowest optical gap reported earlier is 4.11 eV while we have found two nearly degenerate excitations at higher energies of values, 4.83 and 4.87 eV. A low-lying state at an energy of 3.88 eV, which has a small transition dipole appears in the same subspace as of the optical states. This is probably because we have incorporated only one C_2 symmetry axis in our calculations. In DMRG calculations, for computing transition dipole moments we have used average density matrices, obtained from eigenstates of different symmetry subspaces and hence the spatial symmetry is not retained. This could lead to a small transition dipole moment as an artifact for this state (3.88 eV) although

TABLE IV. Lowest triplet state energies obtained in $M_S = 1$ sector and in $M_S = 0$ sector with $\chi_P = -1$ for coronene, ovalene and 1,12-benzoperylene in units of eV.

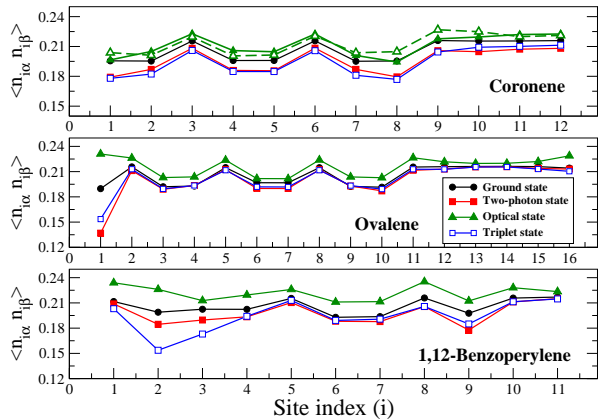|	$M_S = 1$	$M_S = 0, \chi_P = -1$
Coronene	-58.67378	-58.56182
Ovalene	-80.50885	-80.37843
1,12-Benzoperylene	-52.54237	-52.32442

FIG. 3. (Color online) Double occupancy plot with site index for coronene (top panel), ovalene (middle panel) and 1,12-benzoperylene (bottom panel). As all molecules are symmetric about C_2 axis, only half of the molecular sites are plotted, the other half being symmetry equivalent to it. The color scheme for double occupancy in different eigenstates are same in all three panels and are as follows: ground state (black filled circles), lowest two-photon state (red filled square), lowest optical state (green filled triangles) and lowest triplet state (blue open squares). Double occupancy in the other partner of the degenerate optical states in coronene is shown by green broken line with open triangles. Lines connecting data points are given only as a guide to the eye.

this state correspond $e - h$ allowed subspace and if spatial symmetry is not retained strictly we will have a weak transition dipole. On the other hand, the 2.82 eV excitation in coronene is optically forbidden as it belongs to the same e-h symmetry subspace as the ground state. This argument is supported by the fact that this state acquires some intensity on breaking the $e - h$ symmetry by introducing substituents, as can be seen from Table. III. Thus it appears that as in benzene, in coronene the lowest degenerate excitations are pushed up in energy while the higher energy non-degenerate states cross these excitations on incorporating electron-electron interactions. In case of ovalene, we have found the lowest optical gap to be greater than the lowest two-photon gap while reverse ordering of states has been reported earlier. The earlier reported energy gap between the lowest one- and two-photon states as well as that obtained by us are relatively small. The earlier study used interaction parameters optimized to yield experimental gaps in condensed phase while our study employs parameters which are applicable to isolated molecules. In condensed phase the one-photon state will shift more towards the longer wavelength regime than two-photon state, the former being ionic in nature. Thus we expect that the one-photon state will be below the two-photon state for ovalene in solution. The polarization in ovalene in the lowest one-photon state is along the short axis while the higher energy optical excitation is long axis polarized. This is due to the fact that excitons with charge separation along the short axis are more stable than those with separation along the long axis. Indeed, similar polarization for dipole excitations is also found in polyacenes[6].

The lowest triplet state energy in each of the molecules can be calculated in two ways while employing both C_2 and J symmetries – either by calculating the lowest energy state in $M_S = 1$ sector or by calculating the lowest energy state in the $M_S = 0$ space with $\chi_P = -1$. The energies obtained by both calculations are given in Table. IV. It can be observed that the energies obtained in $M_S = 1$ sector calculations are lower. This can be attributed to the larger Hilbert space of the $M_S = 1$ state for a given DMRG cut-off compared to the Hilbert space dimension of the $M_S = 0$ space with $\chi_P = -1$. In fact, the parity symmetry almost bisects the complete direct product space and therefore, the effective size of the

Hilbert space becomes half of that in $M_S = 1$ sector calculation. As DMRG is a variational technique, accuracy increases with the dimension of the Hilbert space and hence, the $M_S = 1$ sector calculations are more accurate.

Spin gap is also a good measure of electronic correlation strength. For a PPP chain, the spin gap can be estimated from the Heisenberg model, with an antiferromagnetic $J \sim 4t^2/U_{PPP}$. This implies that with increasing effective correlation strength, the gap between the lowest singlet state and the lowest triplet state reduces. According to this line of argument, ovalene has the highest effective correlation strength while 1,12-Benzoperylene has the lowest among the molecules sited in Table. II and III.

Substitution by donor-acceptor groups does not seem to have appreciable effect on correlation strength, although, the lifting of electron-hole symmetry allows optical transition to states which are labelled as dipole-forbidden in unsubstituted molecules. The extent of mixing of different symmetry states of the unsubstituted system due to substitution depends on the strength of the donor-acceptor groups. In the present case, the dipole-forbidden $1\,{}^1B_{2u}^+/1\,{}^1B_{3u}^+$ state in unsubstituted coronene becomes symmetry allowed due to substitution and corresponds to the lowest optical state in substituted coronene.

It is evident from above that the effective electron correlation strength is not controlled by the symmetry of the molecule; while coronene is the molecule with highest symmetry (D_{6h}), substitution by donor-acceptor groups
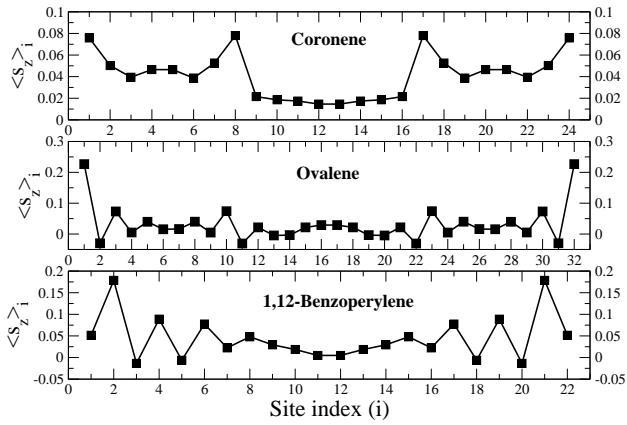
FIG. 4. Spin density plot for coronene (top panel), ovalene (middle) and 1,12-benzoperylene (bottom) in the lowest triplet state. The data points are connected by a line for sake of smooth vision.

lowers the symmetry to C_{2h}, yet, the effective correlation strength in both the systems as indicated by the spin gaps and relative positions of the energy levels, are comparable. Ovalene is also a lower symmetry molecule (D_{2h}) than coronene, but appears to have large effective correlation strength. On the contrary, 1,12-benzoperylene (C_{2v}) being of similar symmetry to substituted coronene, seems to have rather low effective correlation strength compared with the latter.

Spin density at different sites in the lowest triplet state, which is the expectation value of $\langle \hat{S}_i^z \rangle$ in this state is plotted for different molecules in Fig. 4. In the coronene molecule we noted that the spin density is highest at sites 1, 8, 17 and 24 which are all related by symmetry of the molecule. The fractional double occupancies at the above mentioned sites are small (Fig. 3), which is consistent with the higher spin densities at these sites. However, the bond order pattern along the periphery has period four and correspond to $+ = - - = +)_n$ which is unusual as one would expect a quinonoidal structure from the spin density data. On the contrary, the spin densities are well-localized at sites 1 and 32 in ovalene and at 2 and 21 in 1,12-benzoperylene (Fig. 2 and 4). In ovalene and 1,12-benzoperylene, there are many sites with negative spin densities unlike in the case of coronene. Again, we noted that the fractional double occupancy is least at sites with high positive spin densities (Fig. 3). The peripheral bond order in ovalene has period four with kinks at the high spin density sites at the middle of the molecule. Bond 11 and its symmetry partners (Fig. 2) in the interior two benzene rings are rather weak as compared to that in the ground state and we can expect puckering of the structure in the triplet state. In 1,12-benzoperylene also we find bond order pattern with period four on the periphery if we exclude bonds involving the high spin density sites. In substituted coronene, the spin density distribution is not sensitive to the strength of the substituents considered in this study.

We have tabulated the bond order values of different bonds, as indexed in Fig. 2 in lowest energy states of each symmetry subspaces, for all the four molecules studied here. The bond order values are related to bond lengths as indicated by Coulson[20]; bonds with higher bond order value has more double bond character while low value depicts that the bond is primarily a single bond. The repercussion of similar bond order values for different bonds in coronene establishes D_{6h} symmetry of the ground state. This particular symmetry is not retained in the excited states indicating distorted equilibrium structures in these states. In excited states the bonds are symmetric about two in-plane C_2 axes, which bisects the molecule. In two-photon state, a quinonoid structure emerges at the central part of the molecule, while in the doubly degenerate optical states, which have almost similar bond orders and in the lowest triplet state the central benzene ring gets squeezed compared to ground state and its connectivity to the peripheral benzene rings becomes weaker. Similar structures appear even in substituted coronene. Small variation in bond orders for bonds connected to donor or acceptor sites are quite expected as the effective hopping amplitudes for bonds involving these sites will be different from the rest of the molecule. In ovalene, the edge bonds switch their character from double bond to single bond and vice versa in two-photon state and triplet state, relative to those in the ground state. In optical state, the edge bonds become more or less of same character as all the bond orders become nearly equal. Yet, the most notable bond variation in ovalene is for the bonds 11 and 12 and their symmetry partners, which also switch their character like the edge bonds, but in all excited states; other bonds in the inner part of the molecule remain almost invariant. However, the biggest variation in bond order is observed in the lowest triplet state of 1,12-benzoperylene when compared to the ground state bond orders. The Pauli blocking at the sites 2 and 21 converts the bond 1 from a single bond to a double bond. Weakening of neighboring bonds can also be attributed to the Pauli blocking. Bond orders of most of the peripheral and ring bonds become nearly equal while bonds parallel to bond 1 remain approximately same in all states. In the two-photon state, overall expansion of the structure is observed while in the optical state, most significant variation in bond order occurs in the lowermost ring as shown in Fig. 2. The bond order of the weakest bond of the molecule increases both in the two-photon state and the optical state also, but rather small compared to that in the triplet state.

The charge gap of a system is defined as the energy required to remove an electron from a neutral molecule and placing it on another neutral molecule. This process gives rise to two charged species of different charges and can be represented by the reaction[6]:

$$2M \rightarrow P^+ + P^-$$

The charge gap for a system can be calculated by ob-

TABLE V. Bond order for coronene, substituted coronene, ovalene and 1,12-benzoperylene in ground state, lowest two-photon state, lowest optical state and lowest triplet state. The bond indices are according to Fig. 2.

Bond index	Coronene				Substituted coronene				Ovalene				1,12-Benzoperylene			
	$1^1A_g^+$	$2^1A_g^+$ or $2^1B_{1g}^+$	$1^1B_{2u}^-$ and $1^1B_{3u}^-$	$1^3B_{2u}^+$ or $1^3B_{3u}^+$	1^1A_g	2^1A_g	1^1B_u	1^3B_u	$1^1A_g^+$	$2^1A_g^+$ or $2^1B_{1g}^+$	$1^1B_{2u}^-$	$1^3B_{2u}^+$ or $1^3B_{3u}^+$	$1^1A_1^+$	$2^1A_1^+$	$1^1B_1^-$	$1^3B_1^+$
1	0.74	0.64	0.69	0.68	0.74	0.64	0.67	0.70	0.70	0.75	0.74	0.75	0.35	0.42	0.43	0.52
2	0.50	0.52	0.52	0.50	0.50	0.52	0.51	0.49	0.53	0.45	0.49	0.46	0.64	0.57	0.53	0.47
3	0.50	0.51	0.52	0.53	0.50	0.51	0.52	0.54	0.47	0.56	0.52	0.55	0.58	0.55	0.58	0.48
4	0.74	0.67	0.66	0.63	0.74	0.67	0.65	0.62	0.76	0.63	0.71	0.67	0.69	0.65	0.67	0.71
5	0.50	0.45	0.47	0.50	0.50	0.44	0.48	0.50	0.44	0.54	0.47	0.52	0.55	0.54	0.52	0.45
6	0.56	0.46	0.49	0.48	0.56	0.47	0.46	0.47	0.57	0.43	0.53	0.48	0.46	0.50	0.50	0.53
7	0.47	0.56	0.53	0.53	0.50	0.56	0.54	0.54	0.55	0.51	0.53	0.52	0.76	0.67	0.68	0.65
8	0.47	0.43	0.48	0.49	0.46	0.42	0.48	0.49	0.51	0.50	0.50	0.50	0.46	0.49	0.53	0.54
9	0.56	0.58	0.51	0.50	0.56	0.58	0.49	0.51	0.47	0.51	0.49	0.50	0.52	0.53	0.45	0.45
10									0.53	0.54	0.53	0.54	0.72	0.57	0.74	0.73
11									0.52	0.44	0.46	0.45	0.52	0.48	0.50	0.46
12									0.47	0.58	0.55	0.58	0.54	0.46	0.50	0.53
13													0.47	0.56	0.52	0.52
14													0.48	0.45	0.48	0.47
15													0.57	0.43	0.47	0.49

taining the lowest energies in the hole and electron doped systems, and subtracting from their sum the energy of two neutral molecules:

$$E_C(N) = E_{P^+}(N) + E_{P^-}(N) - 2E_M(N)$$

where N is the number of sites in a particular system.

In Hückel picture, the process is same as of photoexcitation and the charge gap will be equal to the optical gap. Long range interactions can alter the picture as the electron-hole pair can get stabilized in a bound state, the exciton. The photoexcitation generally brings the system up to the excitonic state, which can be intramolecular in nature. For complete separation of the electron and hole, so they can move freely, the exciton has to be dissociated and the two charged species should be in the continuum. The energy required to dissociate the exciton leading to freely moving electron and hole is the exciton binding energy. In Table.VI, we have presented

TABLE VI. Charge gap and exciton binding energy in coronene, ovalene and 1,12-benzoperylene in units of eV.

	Charge gap	Exciton binding energy
Coronene	7.05	$2.18 - 2.22$
Ovalene	5.41	2.09
1,12-Benzoperylene	8.21	4.49

the charge gaps and the exciton binding energies for the unsubstituted molecules studied. The exciton binding energies are rather large, comparable for coronene and ovalene and largest for 1,12-benzoperylene. Large exciton binding energies suggest that these molecules cannot be used in solar cell devices.

IV. CONCLUSION

Effective electronic correlation strength in higher-dimensional system is a very subtle parameter which is not only controlled by the one-particle bandwidth but also by the topology of the system. Indeed, correlation plays a crucial part in the relative ordering of the one-photon, two-photon and triplet states. In this article, we have studied the lowest energy level ordering in some peri-condensed polyaromatic systems using the PPP model with standard parameters for sp^2 carbon atoms. We find the energy level ordering to be strongly dependent on the topology of the transfer terms in these molecules. The effective strength of correlation in these molecules are also speculated from the energy level ordering and their energy gaps from the ground state. To enable these studies, we developed a computationally efficient algorithm for symmetry adaptation within the conventional DMRG procedure and obtained energy gaps for several one-photon, two-photon and triplet states in coronene, ovalene, 1,12-benzoperylene and substituted

coronene. We have analyzed the bond order data of the excited states to infer the distortions in their equilibrium geometries while average double occupancy in these states are also computed to understand the effective correlation strength. In the triplet state, we have also calculated spin densities. All these studies show that unlike the linear conjugated systems, the conjugation topology plays an important role besides the interaction parameters.

ACKNOWLEDGMENTS

[1] A. H. Castro Neto, F. Guinea, N. M. R. Peres, K. S. Novoselov, and A. K. Geim, Rev. Mod. Phys. **81**, 109 (2009).

[2] P. R. Wallace, Phys. Rev. **71**, 622 (1947).

[3] K. Schulten and M. Karplus, Chem. Phys. Lett. **14**, 305 (1972); P. Tavan and K. Schulten, Phys. Rev. B **36**, 4337 (1987).

[4] Z. G. Soos and S. Ramasesha, Phys. Rev. B **29**, 5410 (1984); S. Ramasesha and Z. G. Soos, J. Chem. Phys. **80**, 3278 (1984).

[5] K. Tandon, S. Ramasesha, and S. Mazumdar, Phys. Rev. B **67**, 045109 (2003); Z. Shuai, D. Beljonne, R. J. Silbey, and J. L. Brédas, Phys. Rev. Lett. **84**, 131 (2000).

[6] C. Raghu, Y. A. Pati, and S. Ramasesha, Phys. Rev. B **66**, 035116 (2002).

[7] H. Zhao and S. Mazumdar, Phys. Rev. Lett. **93**, 157402 (2004); C. D. Spataru, S. Ismail-Beigi, L. X. Benedict, and S. G. Louie, *ibid.* **92**, 077402 (2004); E. Chang, G. Bussi, A. Ruini, and E. Molinari, *ibid.* **92**, 196401 (2004).

[8] J. W. Patterson, J. Am. Chem. Soc. **64**, 1485 (1942); E. J. Bowen and B. Brocklehurst, J. Chem. Soc. , 3875 (1954); P. J. Stephens, P. N. Schatz, A. B. Ritchie, and A. J. McCaffery, J. Chem. Phys. **48**, 132 (1968); W. R. Dawson and J. L. Kropp, J. Phys. Chem. **73**, 1752 (1969); J. Tanaka, Bull. Chem. Soc. Jpn. **38**, 86 (1965); J. Aihara, K. Ohno, and H. Inokuchi, *ibid.* **43**, 2435 (1970); E. Clar and W. Schmidt, Tetrahedron **33**, 2093 (1977); P. Ehrenfreund, L. d'Hendecourt, L. Verstraete, A. Leger, W. Schmidt, and D. Defourneau, Astron. Astrophys. **259**, 257 (1992); R. Ruiterkamp, T. Halasinski, F. Salama, B. H. Foing, L. J. Allamandola, W. Schmidt, and P. Ehrenfreund, *ibid.* **390**, 1153 (2002); T. Itoh, J. Mol. Spectrosc. **252**, 115 (2008); R. Abouaf and S. Díaz-Tendero, Phys. Chem. Chem. Phys. **11**, 5686 (2009); J. K. Fawcett, "The determination and refinement of the molecular structures of some organic compounds," `http://hdl.handle.net/2429/38382` (1965).

[9] W. E. Moffitt and C. A. Coulson, Proc. Phys. Soc. **60**, 309 (1948).

[10] H. O. Pritchard and F. H. Sumner, Proc. Roy. Soc. A **226**, 128 (1954); R. L. Hummel and K. Ruedenberg, J. Phys. Chem. **66**, 2334 (1962).

[11] M. Hammonds, A. Pathak, and P. J. Sarre, Phys. Chem. Chem. Phys. **11**, 4458 (2009); J. L. Weisman, T. J. Lee, F. Salama, and M. Head-Gordon, The Astrophysical Journal **587**, 256 (2003); O. Birer, P. Moreschini, and K. K. Lehmann, Phys. Chem. Chem. Phys. **10**, 1648 (2008); G. Malloci, G. Mulas, and C. Joblin, Astron. Astrophys. **426**, 105 (2004).

[12] K. Aryanpour, A. Roberts, A. Sandhu, R. Rathore, A. Shukla, and S. Mazumdar, J. Phys. Chem. C **118**, 3331 (2014).

[13] K. Aryanpour, A. Shukla, and S. Mazumdar, J. Chem. Phys. **140**, 104301 (2014); C. Cocchi, D. Prezzi, A. Ruini, M. J. Caldas, and E. Molinari, J. Phys. Chem. A **118**, 6507 (2014).

[14] S. R. White, Phys. Rev. Lett. **69**, 2863 (1992); Phys. Rev. B **48**, 10345 (1993).

[15] S. Ramasesha, S. K. Pati, H. R. Krishnamurthy, Z. Shuai, and J. L. Brédas, Phys. Rev. B **54**, 7598 (1996).

[16] U. Schollwöck, Rev. Mod. Phys. **77**, 259 (2005).

[17] R. Pariser and R. G. Parr, J. Chem. Phys. **21**, 466 (1953); J. A. Pople, Trans. Faraday Soc. **49**, 1375 (1953).

[18] K. Ohno, Theor. Chim. Acta **2**, 219 (1964); G. Klopman, J. Am. Chem. Soc. **86**, 4550 (1964).

[19] S. Ramasesha and Z. Soos, Int. J. Quan. Chem. **25**, 1003 (1984).

[20] C. A. Coulson, Proc. Roy. Soc. A **169**, 413 (1939).